COMMUNICATION

Thermoelectric Generators

ADVANCED
ELECTRONIC
MATERIALS
www.advelectronicmat.de

Flexible Thermoelectric Generators with Ultrahigh Output Power Enabled by Magnetic Field–Aligned Metallic Nanowires

Yani Chen, Minhong He, Junhui Tang, Guillermo C. Bazan, and Ziqi Liang*

Emerging organic–inorganic thermoelectric nanocomposites (TENCs) are promising candidates for the realization of high-performance flexible thermoelectric generators (TEGs), yet there is an absence of effective means to precisely regulate the film morphology of TENCs. Here, the use of a magnetic field to improve thermoelectric performance of solution fabricated n-type metallic TENCs is reported. Of particular relevance is that the magnetic field gives rise to aligned Co nanowires (NWs) within a poly(vinylidene fluoride) (PVDF) matrix. Such oriented TENCs exhibit significantly increased electrical conductivity in comparison to identical nanocomposites that are randomly oriented. As a result, the best power factor of oriented Co NWs (80 wt%)/PVDF TENCs reaches 523 µW m^{-1} K^{-2} at 320 K, which is among the highest reported n-type TENCs. By pairing these n-type TENCs with benchmark p-type poly(3,4-ethylenedioxythiophene)-poly(styrenesulfonate) (PEDOT:PSS) thin films, the fabrication of flexible and planar TEGs that yield a maximum output voltage and power of 26.4 mV and 5.2 µW when $\Delta T = 50$ K, respectively, is reported.

Thermoelectric (TE) energy conversion is regarded as a promising green technology owing to its wide applications in power generation and refrigeration.[1–4] Flexible thermoelectric generators (TEGs) have received increasing attention because they are excellent candidates for the realization of wearable electronics.[5,6] TEGs convert a temperature gradient directly into electrical potential via the Seebeck effect. Such a process is eco-friendly and does not require any moving parts. In this respect, organic and hybrid TE materials stand out due to the unique opportunities they offer in terms of mechanical flexibility, solution processability, facile scalability, and low thermal conductivity.[5]

The performance of TE materials is defined by the dimensionless figure of merit, $zT = S^2\sigma T/\kappa$,[7] where S is the Seebeck coefficient, σ is the electrical conductivity, T is the absolute temperature, and κ is the thermal conductivity including contributions from both phonons (κ_L) and electrons (κ_e). Another equally important parameter is power factor (PF = $S^2\sigma$) that is proportional to the maximum output power.

A typical TEG consists of p- and n-type legs joined at their ends in series, and its performance is determined by the properties of both the components. However, the development of n-type TEs lags behind their p-type analogs. While p-type TE materials, such as poly(3,4-ethylenedioxythiophene)-poly(styrenesulfonate) (PEDOT:PSS)[8–10] and its composites with tellurium nanowires[11,12] or carbon nanotubes (CNTs),[13] can reach PFs > 100 µW m^{-1} K^{-2}, it is rare for n-type counterparts to obta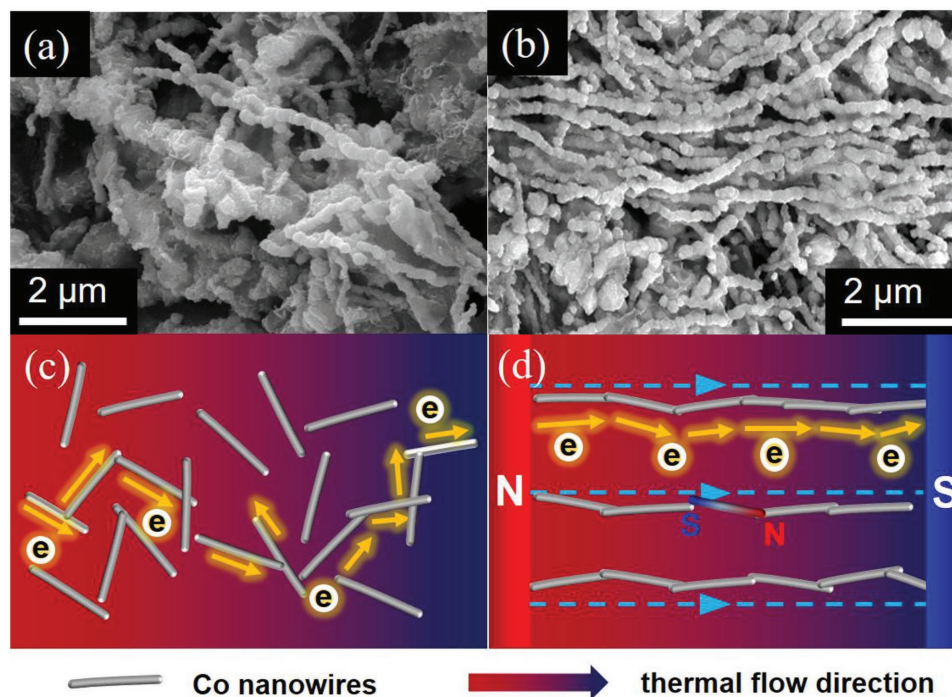in a comparable performance. Considerable efforts have been dedicated to resolve this issue. For instance, Koumoto and co-workers successfully applied electrochemical intercalation and solvent-exchange methods to fabricate the n-type superlattice TiS$_2$/[(hexylammonium)$_x$(H$_2$O)$_y$(dimethylsulfoxide)$_z$], which yielded a high PF of 450 µW m^{-1} K^{-2}.[14] Also, Zhu and co-workers synthesized a metal-containing conducting polymer, poly[K$_x$(Ni-ett)], which delivered an equally high PF of up to 453 µW m^{-1} K^{-2} and an encouraging zT value of 0.3.[15] Subsequently, the same group employed n-type bismuth interfacial doping of thiophene–diketopyrrolopyrrole-based quinoidal (TDPPQ) molecules to obtain a PF of 113 µW m^{-1} K^{-2}.[16] n-Type thermoelectric nanocomposites (TENCs) have been improving rapidly. For example, PEDOT/single-walled CNT (SWCNT) hybrids have been shown to give PFs of up to 1000 µW m^{-1} K^{-2} upon n-doping tetrakis(dimethylamino)ethylene (TDAE).[17] n-Type TENCs based on SWCNTs and amino-substituted perylene diimide (PDINE) or naphthalene diimide (NDINE) displayed the maximum PFs of 112 ± 8 and 135 ± 14 µW m^{-1} K^{-2}, respectively.[18] More recently, we demonstrated that metallic TENCs consisting of Ni nanowires (NWs) embedded within an electrically insulating poly(vinylidene fluoride) (PVDF) matrix generated a notably high σ of 4701 S cm^{-1}, a S of −20 µV K^{-1}, and hence an impressive PF of 200 µW m^{-1} K^{-2} at room temperature.[19] In this respect, insulating PVDF acts to template the interconnectivity of the inorganic NWs without additional electrical contribution. However, the film morphology of solution-casted TENCs remains to be well controlled and provides

Dr. Y. Chen, Dr. M. He, J. Tang, Prof. Z. Liang
Department of Materials Science
Fudan University
Shanghai 200433, China
E-mail: zqliang@fudan.edu.cn
Prof. G. C. Bazan
Department of Chemistry and Biochemistry and Department of Materials Science
University of California at Santa Barbara
CA 93106-9510, USA

The ORCID identification number(s) for the author(s) of this article can be found under https://doi.org/10.1002/aelm.201800200.

ADVANCED
SCIENCE NEWS
www.advancedsciencenews.com

ADVANCED
ELECTRONIC
MATERIALS
www.advelectronicmat.de

Figure 1. Top-view FE-SEM images of Co NWs (80 wt%)/PVDF TENCs and their schematic electron transport: a,c) randomly distributed and b,d) magnetically aligned. "N" and "S" represent the north and south poles of the magnet, respectively.

a unique opportunity for further improving thermoelectric performance. More importantly, as summarized in Table S1 (Supporting Information), most of the state-of-art flexible TE modules are based on CNTs, which required heavy doping to increase electrical conductivity yet inevitably decreased Seebeck coefficient and introduced morphological defects.

In this work, we for the first time utilize the magnetic characteristics of metal NWs to direct the assembly in TENCs through a method that is simple to operate and adds no additional cost. As proof-of-concept, we fabricated Co NWs/PVDF TENCs from solution while applying a magnetic field to selectively orient Co NWs. Such a magnetic method affords anisotropic controllability of individual nanowires, which is yet to be exploited for TENCs. This morphological reorganization leads to significantly increased electrical conductivity from 5648 to 7141 S cm^{-1} and the nearly unchanged Seebeck coefficient, which is much more effective than conventional chemical doping treatments. As a result, the maximum PF up to 520 μW m^{-1} K^{-2} is obtained for the thus aligned Co NWs/PVDF TENCs, which is among the highest achieved for n-type TENCs. Furthermore, by pairing Co NWs/PVDF TENCs with complementary p-type PEDOT:PSS, flexible and planar TE modules containing 10 p–n units were successfully constructed with a maximum output voltage and an output power of 26.4 mV and 5.2 μW, respectively, under a temperature gradient (ΔT) of 50 K. Of a particular note, recent studies have successfully demonstrated the incorporation of inorganic magnetic nanoparticles such as permanent-magnet BaFe$_{12}$O$_{19}$[20] or transition-metal (Fe, Co, or Ni) nanoparticles[21] into Ba$_{0.3}$In$_{0.3}$Co$_4$Sb$_{12}$ matrix. However, they were obtained by ball-milling and sintering without magnetic alignment.

The Co NWs/PVDF TENCs were solution fabricated by mixing Co NWs with PVDF in *N,N*-dimethylformamide (DMF) solvent under mild mechanical stirring, followed by drop-casting onto aluminum molds to generate 80 μm thick thin films. Co NWs/PVDF TENCs with different ratios of Co NWs (i.e., 20, 35, 50, 60, 80 wt%) were prepared. Note that 20, 35, 50, 60, and 80 wt% of Co NWs correspond to 4.7, 9.72, 16.7, 27.1, and 44.5 vol% in the nanocomposites. A magnetic field was applied during the drying process under N$_2$ atmosphere to enforce orientation, as shown in Figure S1 (Supporting Information). **Figure 1**a,b displays the representative top-view field-emission scanning electron microscopy (FE-SEM) images of randomly distributed and magnetically aligned Co NWs/PVDF TENC films. It can be seen that Co NWs assemble into highly ordered domains after applying the magnetic field (Figure 1b). Such well alignment of Co NWs can also be observed in cross-sectional transmission electron microscopy (TEM) images, as shown in Figure S2 (Supporting Information). Most dark dots are evenly dispersed in TENCs with an average diameter of 150–200 nm, which can be assigned to the cross-section of magnetically aligned Co NWs. Only a small amount of different-sized spots exist, as indicated by rectangles and cycles, which can be referred to the tilted and aggregated nanowires, respectively. As a result, the magnetic-aligned sample leads to largely reduced "dead ends" within the metallic network. As schematically illustrated in Figure 1c, these "dead ends" do not contribute to electron transport according to the percolation theory.[22] In contrast, the electrical transport in the magnetically oriented samples can be greatly promoted because it is unidirectional along the desired direction and also possibly reduces the content of Co NWs required to form a percolated network (Figure 1d). We then investigated morphological variations in the nanocomposites as a function of Co NW content. As shown in Figure S3 (Supporting Information), when the ratio of Co NWs is

**ADVANCED
SCIENCE NEWS**
www.advancedsciencenews.com

**ADVANCED
ELECTRONIC
MATERIALS**
www.advelectronicmat.de

increased from 20, 35, 50, 65 to 80 wt%, the percolated network is gradually formed, which is consistent with our previous report.[19] Figure S4 (Supporting Information) shows that these films are highly flexible, thereby providing opportunities to reconfigure into a variety of shapes relevant for different applications. TENC samples were further analyzed by X-ray diffraction (XRD) measurement. As shown in Figure S5 (Supporting Information), one observes three strong diffraction peaks at 44.5°, 51.8°, and 76.4°, corresponding to the (111), (200), and (220) reflection planes of Co, respectively (JCPDS No. 04-0850). In addition, the intensity of these diffraction peaks increases when the Co content increases from 20 to 80 wt%. The absence of diffraction peaks at 37.2°, 43.2°, 62.8°, 75.3°, and 79.3° indicates the absence of CoO, which would otherwise strongly reduce electrical conductivity.

The room-temperature average TE properties of the Co NWs/PVDF TENCs as a function of Co content are presented in **Figure 2**. Note that both σ and S are compared between random and oriented samples, in the latter of which the measurement was conducted along the direction of magnetic field. As the Co ratio is increased from 20 to 80 wt%, σ values of both the samples exhibit an exponential increase, in accordance with percolation theory.[23] It is worth noting that σ of the oriented samples reaches the highest value of 7141 S cm^{-1} when the Co NW content reaches 80 wt%, and is much higher than that measured for the random one (5648 S cm^{-1}) (Figure 2a). We attribute the increase in σ to better interconnection within Co NW networks as a result of the alignment by the magnetic field, as indicated in Figure 1. The S of all the samples are negative, indicating n-type characteristics. It is also worth noting that there is little difference between the S of these random and oriented samples, suggesting that the magnetic field treatment has little noticeable effect on S (Figure 2b). Interestingly, the absolute S is progressively increased from 12 to 25 μV K^{-1} as the Co content is increased from 20 to 80 wt%, approaching that of neat Co (30 μV K^{-1}). This behavior is analogous to that observed in Ni NWs/PVDF TENCs,[19] which can be explained by the interplay between the intrinsic S of Co and that from the junctions between connected NWs.[23] As a result, the maximum PF of 432 μW m^{-1} K^{-2} is obtained at 80 wt% for the oriented samples (Figure 2c).

To rationalize the influence of magnetic field on TE performance, we conducted temperature-dependent TE measurements on three types of samples—random and oriented along both parallel ($\parallel$) and perpendicular ($\perp$) directions relative to the applied magnetic field. **Figure 3** shows the temperature dependences of average TE properties of the optimal Co (80 wt%)/PVDF TENCs in the range of 300–380 K. In general, σ exhibits a slow descending tendency over temperature, which is typical of metallic behavior due to the enhanced electron scattering. Moreover, it is evident that σ follows such a trend that $\sigma_{\parallel} > \sigma_{random} > \sigma_{\perp}$, in good agreement with the proposed schematics of electron transport in Figure 1c,d. Furthermore, S of all the three samples are temperature insensitive and maintains a value of -25 μV K^{-1}, which is beneficial for practical applications. Consequently, the maximum PF$_{\parallel}$ of oriented TENCs reaches 523 μW m^{-1} K^{-2} at 320 K, which is greater than that of both the random (309 μW m^{-1} K^{-2}) and perpendicular (212 μW m^{-1} K^{-2}) ones, and is also among the highest values
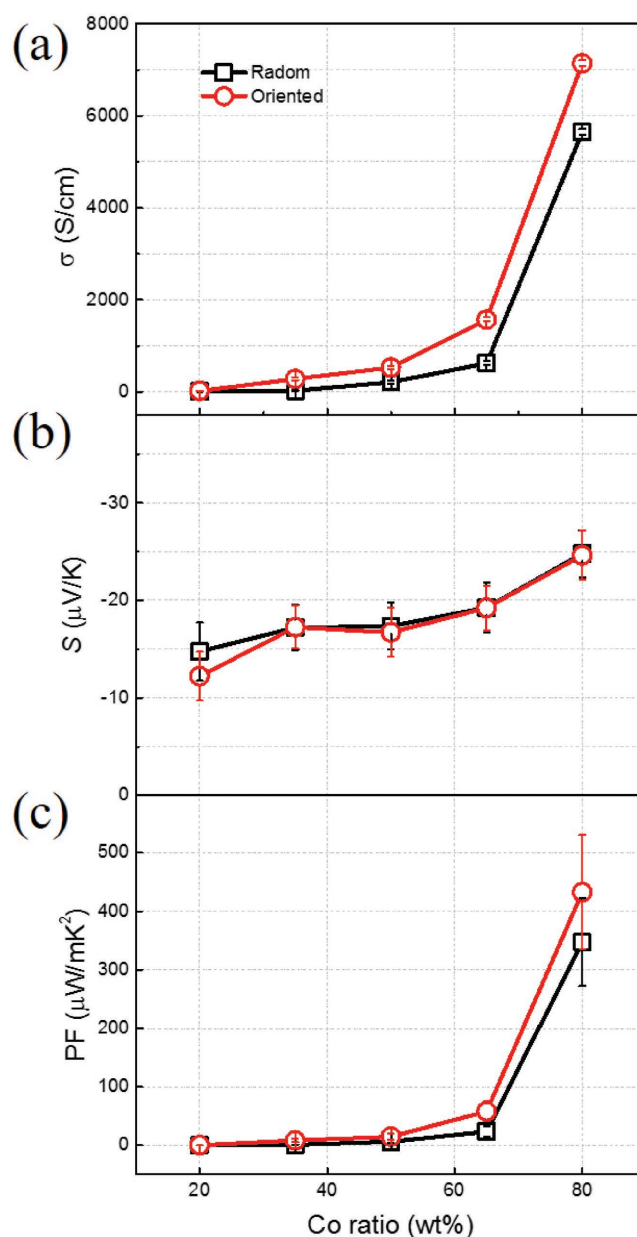
Figure 2. Average TE performance of Co NWs/PVDF TENCs as a function of the Co content at room temperature: a) electrical conductivity, b) Seebeck coefficient, and c) power factor.

reported thus far for n-type TENCs. Furthermore, we performed the bending test on the above optimal sample under a radius of as low as 13.5 mm. As shown in Figure S6 (Supporting Information), after 100 bending cycles, the σ, S, and PF can still maintain 93.5%, 93.2%, and 82.0% of their initial values, respectively, thus holding huge potential for flexible TE devices.

Finally, we demonstrated the fabrication of a flexible and planar TEG device by pairing n-type Co NWs/PVDF TENCs with p-type commercial PEDOT:PSS (PH1000) thin films. The σ, S, and PF of PH1000 were measured to be 200.1 S cm^{-1}, 20.6 μV K^{-1}, and 8.5 μW m^{-1} K^{-2}, respectively. **Figure 4a** displays a photograph of the TEG module consisting of 10 p–n
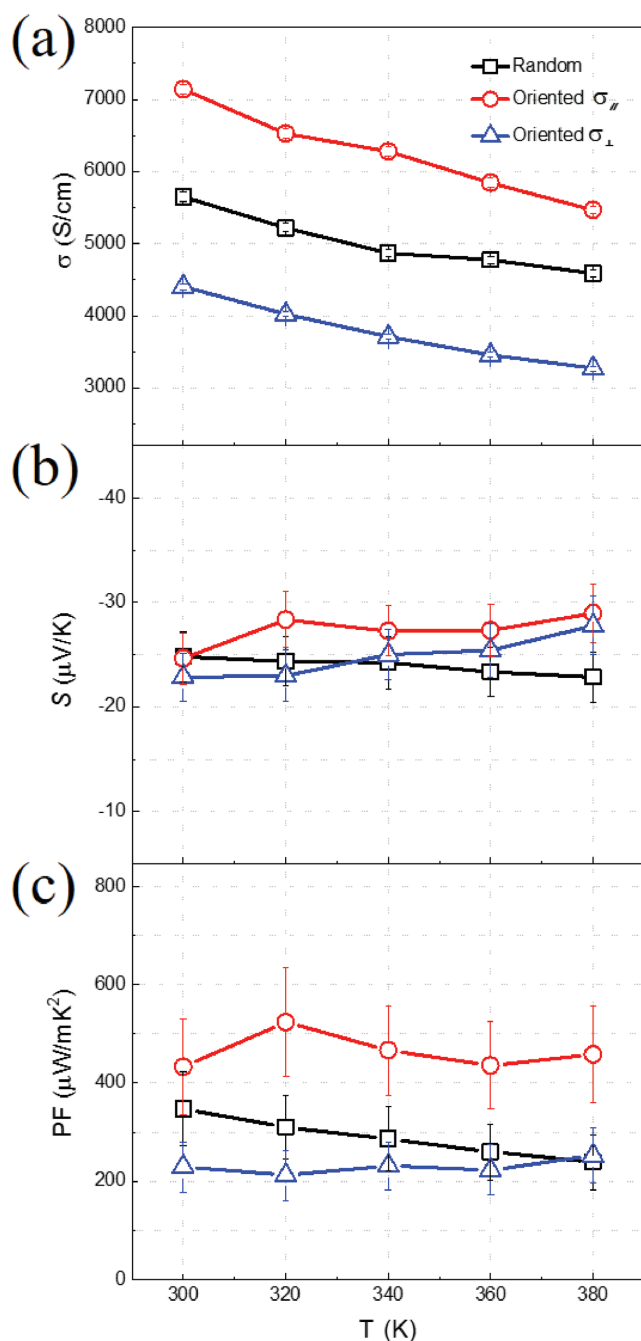
Figure 3. Temperature dependences of average TE properties of the optimal Co NWs (80 wt%)/PVDF TENCs: a) electrical conductivity, b) Seebeck coefficient, and c) power factor.

units. The 20 legs were cut into rectangular strips with an average size of $12.0 \times 5.0 \times 0.06$ and $12.0 \times 3.0 \times 0.08$ mm^3 for p- and n-legs, respectively. The legs were then attached to a flexible polyimide (PI) substrate and interconnected by using Ag paste. To evaluate the power generation characteristics of these TE modules, a home-made system was utilized. As shown in Figure S7 (Supporting Information), the TEG is sandwiched between two copper plates, in which the temperature difference was created by heating one copper plate to $T1$ and cooling

the other to $T2$ via semiconductor chilling plate. Both $T1$ and $T2$ were detected by thermocouples, as indicated by the green cycles. Figure 4b shows the output voltage of the TEG as a function of a steady-temperature gradient, $\Delta T = T1 - T2$. The theoretical voltage (V_{TH}) is determined by Equation (1)[18]

$$V_{TH} = n \times \left(S_n + S_p \right) \times \Delta T \tag{1}$$

where n, S_n, S_p are the number of the p–n junctions, absolute Seebeck coefficients of n- and p-type components, respectively. As ΔT is elevated from 10 to 50 K, the output voltage increases linearly from 6.9 to 26.4 mV, which is comparable to the V_{TH} (V) and is among the highest values for previously reported hybrid TEGs.[24–26] Figure 4c presents the output power of the TEG as a function of both ΔT and load resistance. As ΔT is increased from 10 to 50 K, the output power increased proportionally. As a result, a maximum power output of 5.2 µW is obtained when $\Delta T = 50$ K and the load resistance is 32.7 Ω, corresponding to the power output density of 1 µW mg^{-1} and 0.26 µW cm^{-2} after dividing the weight and the area occupied by p–n legs, respectively (Figure 4d). These values are higher than those of previous reports in CNT-based flexible TEGs (Table S1, Supporting Information).[24–26] A remarkably high power density of 660 µW cm^{-2} is obtained when calculating from the leg cross-sectional area where the carriers pass through. Movie S1 (Supporting Information) shows that this TEG generates an output voltage of 1.2 mV by the touch of fingertips at 25 °C, which holds excellent promise for portable electronic gadgets such as smart watches, glasses, and pacemakers.

We anticipate that higher output power density can be achieved if 1) the p-type materials are properly chosen to well match with n-type counterparts in electrical performance—in this work, both σ and S of benchmark PEDOT:PSS are largely inferior to those of n-type Co NWs/PVDF TENCs, or 2) more legs are either serially connected or folded. Another point worth noting is that the above-mentioned load resistance (32.7 Ω) is approximate to the total internal resistance of our TEG, which consists of both the electrical resistance of these 10 pairs of legs and the contact resistance. The former can be calculated by Equation (2)

$$R = n \times \left(\frac{1}{\sigma_p} \times \frac{l_p}{A_p} + \frac{1}{\sigma_n} \times \frac{l_n}{A_n} \right) \tag{2}$$

where l, A are the length and the cross-sectional area, respectively. As a result, the total resistance of p- and n-legs is 20.7 Ω, including 20.0 and 0.67 Ω for p- and n-legs, respectively. The contact resistance is then subtracted to be ≈12 Ω, which can be further reduced by optimizing the welding process of neighboring legs.

In conclusion, we have successfully demonstrated that a magnetic field is a simple morphology-directing tool to improve thermoelectric characteristics of solution-processed n-type Co NWs/PVDF TENCs. Upon applying the magnetic field, the electrical conductivity exhibits strong magnetic anisotropy (i.e., $\sigma_\parallel > \sigma_{random} > \sigma_\perp$), while the Seebeck coefficient shows little dependence. At the Co NW content of 80 wt%, both reach the highest values of 7141 S cm^{-1} and 25 µV K^{-1}, respectively,
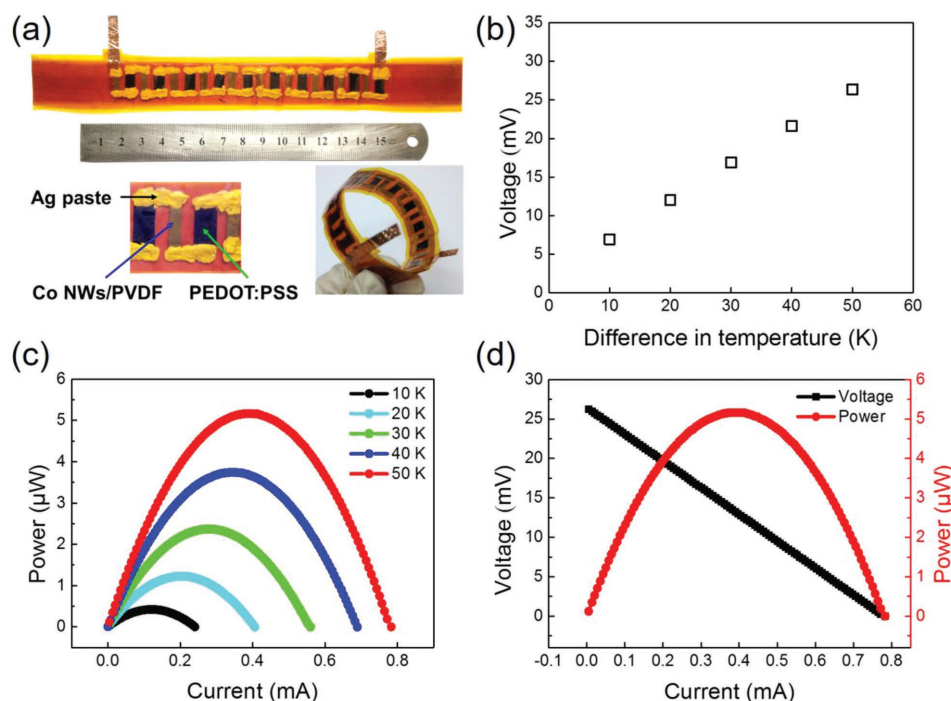
Figure 4. Performance of compact-designed TE modules. a) Photographs of flexible TE module consisting of 10 p–n units. b) Open-circuit voltage and c) output power as a function of temperature gradient (ΔT). d) The voltage–current and power–current curves of the module at the hot-side temperature of 330 K with a temperature difference of 50 K.

at room temperature, due to the well alignment of Co NWs in PVDF matrix. A PF of 520 µW m^{-1} K^{-2} is thus obtained, which is among the highest for n-type TENCs reported thus far. A planar TEG was then fabricated, which comprised of 10 pairs of these n-type TENCs and p-type PEDOT:PSS thin films. Under a temperature gradient of 50 K, the maximum output voltage and power achieve 26 mV and 5.2 µW, respectively. This work manifests emerging opportunities for using novel processing techniques that allow the optimization of electron and phonon transport channels in TENCs.

Experimental Section

Chemicals and Materials: All the chemicals used in the experiments were purchased and used without further purification, including Co NWs (JCNANO Tech Co., Ltd.), PVDF (weight-average molecular weight = 900 kDa, Arkem, Ltd.), DMF (J&K Scientific, Ltd.), and Co nanowires (Nanjing Jicang Nano Technology Co., Ltd.).

Fabrication of Co NWs/PVDF TENCs: PVDF (0.1 g) was first dissolved into DMF (0.9 g) in a 50 mL flask under vigorous stirring at 70 °C for 3 h. Subsequently, different quantities of Co NWs at 20, 35, 50, 65, and 80 wt% were dispersed into the PVDF solution under mild mechanical stirring at room temperature over a period of 1 h. Co NWs/PVDF TENCs were obtained by drop-casting the mixture solution into aluminum molds inside a N$_2$-filled glovebox, followed by drying at 40 °C overnight. For the oriented samples, the mold was then placed on a heated plate under a controllable magnetic field with strength of 23 mT. The resulting TENC films were subsequently peeled off from the aluminum molds and pressed under 10 MPa for 2 min.

Characterization and Measurements: Electrical properties of the nanocomposites were measured in the temperature range of 280–380 K by using a custom-built apparatus according to the previous report.[19] A four-probe technique was used to measure electrical conductivity on a multimeter (Keithley 2010) and a source meter (Keithley 2400). The Seebeck coefficient was measured by heating one resistor block while simultaneously measuring the generated temperature gradient (ΔT) and thermoelectric voltage (ΔV). Field-emission scanning electron microscopy images were acquired on JEOL JSM-6701F at an accelerating voltage of up to 30 kV. X-ray diffraction pattern data for 2θ values were collected with a Bruker AX D8 Advance diffractometer with nickel-filtered Cu Kα radiation ($\lambda = 1.5406$ Å).

Supporting Information

Supporting Information is available from the Wiley Online Library or from the author.

Conflict of Interest

The authors declare no conflict of interest.

[1] F. J. DiSalvo, *Science* **1999**, *285*, 703.

[2] L. E. Bell, *Science* **2008**, *321*, 1457.

[3] M. S. Dresselhaus, G. Chen, M. Y. Tang, R. Yang, H. Lee, D. Wang, Z. Ren, J.-P. Fleurial, P. Gogna, *Adv. Mater.* **2007**, *19*, 1043.

[4] G. J. Snyder, E. S. Toberer, *Nat. Mater.* **2008**, *7*, 105.

[5] Y. Chen, Y. Zhao, Z. Liang, *Energy Environ. Sci.* **2015**, *8*, 401.

[6] T. Zhang, K. Li, J. Zhang, M. Chen, Z. Wang, S. Ma, N. Zhang, L. Wei, *Nano Energy* **2017**, *41*, 35.

[7] D. M. Rowe, *Thermoelectrics Handbook: Macro to Nano*, CRC Press, Boca Raton, FL **2005**.

[8] H. Park, S. H. Lee, F. S. Kim, H. H. Choi, I. W. Cheong, J. H. Kim, *J. Mater. Chem. A* **2014**, *2*, 6532.

[9] T. Park, C. Park, B. Kim, H. Shin, E. Kim, *Energy Environ. Sci.* **2013**, *6*, 788.

[10] Z. Fan, P. Li, D. Du, J. Ouyang, *Adv. Energy Mater.* **2017**, *7*, 1602116.

[11] M. Culebras, A. M. Igual-Muñoz, C. Rodríguez-Fernández, M. I. Gómez-Gómez, C. Gómez, A. Cantarero, *ACS Appl. Mater. Interfaces* **2017**, *9*, 20826.

[12] E. J. Bae, Y. H. Kang, C. Lee, S. Y. Cho, *J. Mater. Chem. A* **2017**, *5*, 17867.

[13] M. Culebras, C. Cho, M. Krecker, R. Smith, Y. Song, C. M. Gómez, A. Cantarero, J. C. Grunlan, *ACS Appl. Mater. Interfaces* **2017**, *9*, 6306.

[14] C. Wan, X. Gu, F. Dang, T. Itoh, Y. Wang, H. Sasaki, M. Kondo, K. Koga, K. Yabuki, G. J. Snyder, R. Yang, K. Koumoto, *Nat. Mater.* **2015**, *14*, 622.

[15] Y. Sun, L. Qiu, L. Tang, H. Geng, H. Wang, F. Zhang, D. Huang, W. Xu, P. Yue, Y. S. Guan, F. Jiao, Y. Sun, D. Tang, C. Di, Y. Yi, D. Zhu, *Adv. Mater.* **2016**, *28*, 3351.

[16] D. Huang, C. Wang, Y. Zou, X. Shen, Y. Zang, H. Shen, X. Gao, Y. Yi, W. Xu, C. Di, D. Zhu, *Angew. Chem., Int. Ed.* **2016**, *55*, 10672.

[17] H. Wang, J.-H. Hsu, S.-I. Yi, S. L. Kim, K. Choi, G. Yang, C. Yu, *Adv. Mater.* **2015**, *27*, 6855.

[18] G. Wu, Z.-G. Zhang, Y. Li, C. Gao, X. Wang, G. Chen, *ACS Nano* **2017**, *11*, 5746.

[19] Y. Chen, M. He, B. Liu, G. C. Bazan, J. Zhou, Z. Liang, *Adv. Mater.* **2017**, *29*, 1604752.

[20] W. Zhao, Z. Liu, Z. Sun, Q. Zhang, P. Wei, X. Mu, H. Zhou, C. Li, S. Ma, D. He, P. Ji, W. Zhu, X. Nie, X. Su, X. Tang, B. Shen, X. Dong, J. Yang, Y. Liu, J. Shi, *Nature* **2017**, *549*, 247.

[21] W. Zhao, Z. Liu, P. Wei, Q. Zhang, W. Zhu, X. Su, X. Tang, J. Yang, Y. Liu, J. Shi, Y. Chao, S. Lin, Y. Pei, *Nat. Nanotechnol.* **2017**, *12*, 55.

[22] T. Nakayama, K. Yakubo, R. L. Orbach, *Rev. Mod. Phys.* **2008**, *66*, 381.

[23] B. Liu, T. Lu, B. Wang, J. Liu, T. Nakayama, J. Zhou, B. Li, *Appl. Phys. Lett.* **2017**, *110*, 113102.

[24] C. J. An, Y. H. Kang, H. Song, Y. Jeong, S. Y. Cho, *J. Mater. Chem. A* **2017**, *5*, 15631.

[25] H. Im, T. Kim, H. Song, J. Choi, J. S. Park, R. Ovalle-Robles, H. D. Yang, K. D. Kihm, R. H. Baughman, H. H. Lee, T. J. Kang, Y. H. Kim, *Nat. Commun.* **2016**, *7*, 10600.

[26] W. Zhou, Q. Fan, Q. Zhang, L. Cai, K. Li, X. Gu, F. Yang, N. Zhang, Y. Wang, H. Liu, W. Zhou, S. Xie, *Nat. Commun.* **2017**, *8*, 14886.

1800200 (6 of 6)